

RESEARCH ARTICLE

Symmorphosis and the insect respiratory system: allometric variation

Edward P. Snelling^{1,*}, Roger S. Seymour¹, Sue Runciman², Philip G. D. Matthews³ and Craig R. White³

¹School of Earth and Environmental Sciences, University of Adelaide, South Australia 5005, Australia, ²Anatomy and Histology, Flinders University of South Australia, South Australia 5001, Australia and ³School of Biological Sciences, University of Queensland, St Lucia, Queensland 4072, Australia

*Author for correspondence (edward.snelling@adelaide.edu.au)

SUMMARY

Taylor and Weibel's theory of symmorphosis predicts that structures of the respiratory system are matched to maximum functional requirements with minimal excess capacity. We tested this hypothesis in the respiratory system of the migratory locust, *Locusta migratoria*, by comparing the aerobic capacity of the jumping muscles with the morphology of the oxygen cascade in the hopping legs using an intraspecific allometric analysis of different body mass (M_b) at selected juvenile life stages. The maximum oxygen consumption rate of the hopping muscle during jumping exercise scales as $M_b^{1.02 \pm 0.02}$, which parallels the scaling of mitochondrial volume in the hopping muscle, $M_b^{1.02 \pm 0.08}$, and the total surface area of inner mitochondrial membrane, $M_b^{0.99 \pm 0.10}$. Likewise, at the oxygen supply end of the insect respiratory system, there is congruence between the aerobic capacity of the hopping muscle and the total volume of tracheoles in the hopping muscle, $M_b^{0.99 \pm 0.16}$, the total inner surface area of the tracheoles, $M_b^{0.99 \pm 0.16}$, and the anatomical radial diffusing capacity of the tracheoles, $M_b^{0.99 \pm 0.18}$. Therefore, the principles of symmorphosis are upheld at each step of the oxygen cascade in the respiratory system of the migratory locust.

Supplementary material available online at <http://jeb.biologists.org/cgi/content/full/214/19/3225/DC1>

Key words: allometry, anatomical diffusing capacity, insect, locust, mitochondria, stereology, symmorphosis, tracheal system.

INTRODUCTION

In 1981, Taylor and Weibel, together with their co-workers, introduced the theory of symmorphosis. The principle was defined as the 'state of structural design commensurate to functional needs resulting from regulated morphogenesis, whereby the formation of structural elements is regulated to satisfy but not exceed the requirements of the functional system' (Taylor and Weibel, 1981). The assertion that each step in a biological system is quantitatively matched to the overall maximum functional task of the system is essentially an optimality theory, which was motivated by the belief that animals are built economically because maintaining superfluous structure is energetically expensive (Weibel et al., 1981a).

In a seminal series of papers, Taylor and Weibel tested their theory on the respiratory system of mammals. First, the functional capacity of the respiratory system was determined by measuring the maximum oxygen consumption rate of mammals during exercise of progressive increasing intensity (Seeherman et al., 1981). Next, a number of structural variables crucial in the delivery and consumption of oxygen during exercise were morphometrically quantified (Gehr et al., 1981; Hoppeler et al., 1981a; Hoppeler et al., 1981b; Mathieu et al., 1981; Weibel et al., 1981b). The effect of body mass on the maximum oxygen consumption rate of mammals and the amount of respiratory structure they possess was expressed as an allometric equation, $y = aM_b^b$, where y is the variable of interest, a is the coefficient, M_b is body mass and b is the scaling exponent. Taylor and Weibel predicted that if their theory of symmorphosis holds for the mammalian respiratory system, then maximum oxygen uptake should scale with an exponent (b) that is statistically indistinguishable from the exponents derived for each of the structural variables (Taylor and Weibel, 1981). They found that maximum oxygen consumption rate scales with body mass with

an exponent of 0.80 (Taylor et al., 1981), and that this is congruent with the allometric scaling of mitochondrial volume in the diaphragm and locomotory muscles, $b=0.80$ to 0.82 (Mathieu et al., 1981). It was also established that total capillary length in selected muscles scales roughly parallel with aerobic capacity, $b=0.86$ to 0.91 , but because of scatter in the data it was not possible to determine whether the slopes were statistically similar (Hoppeler et al., 1981b; Weibel et al., 1981a). Interestingly, the anatomical diffusing capacity of the lung was found to scale with an exponent, $b=0.99$, significantly steeper than that derived for maximum oxygen consumption rate, which means that larger mammals appear to possess excess lung structure (Gehr et al., 1981). It was suggested that larger mammals may have a lower alveolar pressure head for diffusion and, therefore, require a greater pulmonary diffusing capacity to transfer oxygen from the lungs to the blood at the same rate as smaller mammals (Gehr et al., 1981). In contrast, the pulmonary anatomical diffusing capacity of birds appears to be symmorphic, both phylogenetically and ontogenetically (Canals et al., 2011; Runciman et al., 2005; Seymour et al., 2004; Seymour et al., 2008).

Since its conception, symmorphosis has received the support of a number of workers who view the optimal design idea as a useful null hypothesis of biological design on which to base analytical studies (Diamond, 1992; Suarez, 1996). Where these simple economy-based expectations break down, an opportunity arises to analyse the reasons for such a breakdown (Diamond, 1992). However, symmorphosis has also evoked criticism, especially from evolutionary biologists, who argue that natural selection leads to adequate or sufficient design but not optimal or symmorphic design (Dudley and Gans, 1991; Garland, 1998; Garland and Huey, 1987; Smith, 1978). They argue that symmorphosis is not an inevitable outcome because environmental unpredictability means that

evolutionary selective forces vary too much in space and time to produce a structure that is functionally optimal (Dudley and Gans, 1991). It is suggested that symmorphosis-like matching between structure and function may only ever be realised when the selective forces influencing design have either been static for a long time (Dudley and Gans, 1991) or when selective pressures have been directed towards extreme performance (Jones and Lindstedt, 1993). Criticism of symmorphosis is supported by a number of instances in which animals appear to be in possession of unnecessary structure. Not only does the mammalian lung appear to have an excess capacity (Canals et al., 2010; Gehr et al., 1981; Hsia et al., 1992; Karas et al., 1987), but excess structure may also exist at oxygen delivery steps further downstream. For example, maximum oxygen uptake in athletic humans, racehorses and mice increases under hyperoxic conditions (Gębczyński and Konarzewski, 2011; Jones and Lindstedt, 1993; Powers et al., 1989), which suggests that in some animals at least, the mitochondria have an aerobic reserve that is never fully exploited.

Whether there are physiological or adaptive explanations for instances where symmorphosis does not hold is open to debate, but first it is worth considering two other factors important in animal design. Firstly, it is likely that many physiological systems have a built-in safety margin, analogous to the safety margin engineers build in to bridges, buildings and elevators. If a structure has no safety margin, then it is at risk of breakage when its performance approaches maximum. For example, the cardiovascular system of racehorses has been artificially selected for high oxygen flux to the extent that the safety margin for pulmonary blood pressure has been significantly compromised, and when physically exerted some horses experience pulmonary bleeding (Pascoe et al., 1981). The second point worth considering is that some structures in the body are multifunctional and this can complicate the interpretation of results. For example, the design of the cardiovascular system could be geared towards oxygen delivery, or it could reflect some other physiological requirement, such as substrate delivery, lactate removal, carbon dioxide removal, pH regulation or heat dispersal (Dudley and Gans, 1991; Garland and Huey, 1987). Clearly, some systems offer a more suitable model on which to test for symmorphosis design. The insect respiratory system appears to be a case in point.

In insects, oxygen delivery occurs along a series of steps (Hartung et al., 2004; Schmitz and Perry, 1999). First, atmospheric oxygen enters the air-filled tubes of the insect's tracheal system through small pores located along its lateral margins, called spiracles. It then moves in the gas phase through a branching system of successively smaller tracheae, before arriving at the terminal tracheoles. Here, it exits the tracheal system and diffuses across the tracheal cuticle and epidermal layers (Fig. 1) before diffusing into tissue where it is used by mitochondria to oxidise substrate to produce ATP for work. Carbon dioxide produced by the respiring cells does not take the exact same path as oxygen in reverse. Because of its greater solubility in tissue and haemolymph, some carbon dioxide may be temporarily retained in the tissue before diffusing into tracheae or passing directly through the integument (Bridges and Scheid, 1982). In some stick insects, for example, up to 25% of carbon dioxide is expelled directly across the exoskeleton (Wigglesworth, 1965). As such, a system capable of bringing an adequate supply of oxygen to the tissues should also suffice to remove carbon dioxide (Chapman, 1998; Schmitz and Perry, 1999).

The primary function of the insect tracheal system, therefore, is to deliver oxygen to the mitochondria, which makes it an ideal model on which to test for symmorphosis. However, there are other characteristics that make it appealing. Oxygen flux through the insect

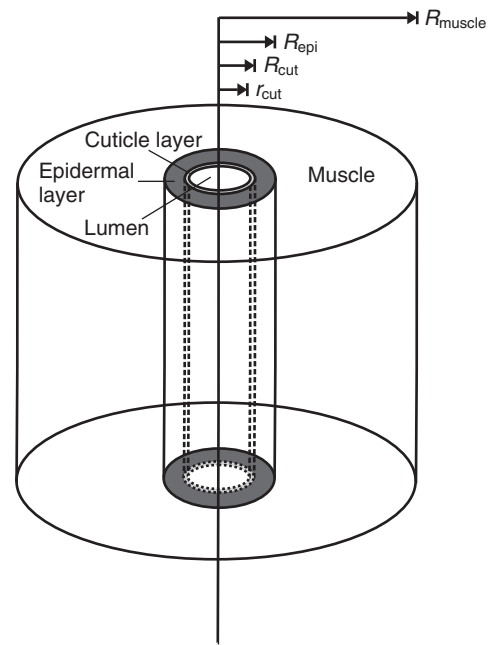


Fig. 1. Krogh's cylindrical model for radial diffusion was originally devised for the diffusion of oxygen out of a vertebrate capillary and into the surrounding muscle. Here we have adapted this and applied it to an insect tracheole. r_{cut} is the mean radius of the tracheole to the inner surface of the cuticle layer (μm), R_{cut} is the mean radius of the tracheole to the outer surface of the cuticle layer (μm), R_{epi} is the mean radius of the tracheole to the outer surface of the epidermal layer (μm) and R_{muscle} is the radius of the mean transverse area of muscle serviced by each tracheole (μm) [after Kreuzer (Kreuzer, 1982)]. Not drawn to scale.

respiratory system is higher than in any other animal group (Sacktor, 1976; Suarez, 2000), and so the selective pressure for optimal design has likely been strong (Jones and Lindstedt, 1993). The high metabolic scope of insects also means that the oxygen requirements of the exercising muscle greatly exceeds metabolism in the remaining tissues, and this makes the work due to exercise easier to quantify. Furthermore, insect locomotory muscles are often easy to identify and thus analyse without including non-locomotory tissues. For example, hopping in locusts is performed by just two muscles contained within each metathoracic femur. Hopping is also entirely aerobic after 2 min of exercise (Kirkton et al., 2005), and for the purpose of an allometric study of symmorphosis, the fact that locust body mass increases more than 30-fold from first to fifth instar is also a key advantage.

The aim of this study was to test whether the respiratory system of the migratory locust, *Locusta migratoria*, is designed according to the economical principles of symmorphosis. To achieve this, allometric variation in the structural properties of the locust respiratory system in the hopping femurs was quantified and compared with the maximum functional rate at which oxygen flows through the system during intense hopping exercise in first, third and fifth instar juveniles. Earlier respirometry showed that the aerobic capacity of the hopping muscle ($\dot{M}_{\text{MO}_2, \text{juv}, \text{hop}}$) scales throughout juvenile locust development according to the allometric equation $\dot{M}_{\text{MO}_2, \text{juv}, \text{hop}} = 103 M_b^{1.02 \pm 0.02} \mu\text{mol O}_2 \text{h}^{-1}$ at 35°C ($r^2 = 0.98$, $N = 145$) (Snelling et al., 2011). If the theory of symmorphosis holds for the insect respiratory system, then similar scaling exponents should also exist for mitochondrial volume, mitochondrial inner membrane surface area, tracheal volume, tracheal surface area and tracheal diffusing capacity in the juvenile locust hopping muscle.

MATERIALS AND METHODS

Animals

Gregarious-phase locusts *Locusta migratoria* (Linnaeus 1758) were reared at $33 \pm 1^\circ\text{C}$, under a 12 h:12 h light:dark cycle, with *ad libitum* access to seedling wheatgrass and wheat germ, as previously described (Snelling et al., 2011). The developmental stage of each locust was determined based on instar-specific differences in wing morphology. Newly moulted individuals were transferred into separate plastic terraria with other locusts of the same age. Morphometric quantification of the metathoracic femur (hopping leg femur) was conducted on locusts in their first, third and fifth instar life stages. Three insects were used from each life stage ($N=9$ individuals). Insects were measured 3–4 days post-moult to provide sufficient time for the exoskeleton to stiffen while minimising compression of the tracheal system due to growth (Greenlee and Harrison, 2004; Queathem, 1991). Locusts were fasted for 6–10 h prior to tissue fixation, consistent with earlier respirometry experiments (Snelling et al., 2011).

Specimen preparation

The procedure used to dissect and fix locust tissue was modified based on the methods of previous electron-microscopy studies of insects and spiders (Biserova and Pfluger, 2004; Hartung et al., 2004; Kohnert et al., 2004; Schmitz and Perry, 2002a; Schmitz and Perry, 2002b). The large extensor tibialis muscle and the smaller flexor tibialis muscle, which are used during hopping locomotion, constitute the entire muscle mass of the metathoracic femur (Bennet-Clark, 1975; Gabriel, 1985a; Gabriel, 1985b) and were identified from published illustrations (Albrecht, 1953).

Locusts were first cold anaesthetised for 20 min in a refrigerator at 4°C . They were then weighed to 0.1 mg on an analytical balance (AE163, Mettler, Greifensee, Switzerland). Both metathoracic femurs on each locust were then carefully removed with angled spring scissors. Each femur was weighed to 0.1 mg before being sliced along the transverse plane into pieces of equal length using a razor. Femurs from first instar locusts were sliced into three pieces, third instar femurs were sliced into six pieces, and fifth instar femurs were sliced into 12 pieces. Each piece of femur tissue was sequentially numbered proximally to distally and labelled left or right. The pieces were immediately immersed into a chemical fixative solution of 2.5% glutaraldehyde and 2% formaldehyde in 0.2 mol l^{-1} phosphate buffer, pH 7.4, and left overnight in a refrigerator at 4°C . On the second day, each piece was given a series of buffer rinses. The first rinse was 20 min, followed by four 60 min rinses. This was followed by three 20 min distilled water rinses, and then the tissue was placed into a 1% aqueous solution of osmium tetroxide for secondary fixation and left overnight at room temperature. On the third day, each piece was given five 20 min rinses in distilled water and then placed into a 2% aqueous solution of uranyl acetate and left overnight at room temperature. On the fourth day, the pieces were given four 20 min rinses in distilled water and then dehydrated in ethyl alcohol in 10% incremental steps from 50 to 80%, each for 20 min. The tissue was then further dehydrated in consecutive 20 min immersion in 90% ethanol ($2\times$), 100% ethanol ($2\times$) and finally pure propylene oxide ($2\times$). Following dehydration, the samples were incrementally infiltrated with embedding resin (Durcupan, Fluka, Buchs, Switzerland) at ratios of 3:1, 2:2 and 1:3 (propylene oxide to resin), respectively, each for a duration of 60 min, and then left overnight at room temperature in pure resin. On the fifth day, each piece was aligned longitudinally and in a proximal to distal orientation in individually labelled embedding moulds, where they were covered with pure embedding resin and left to polymerise in a 70°C oven for 48 h.

Light microscopy

The procedure for sampling the embedded hopping muscle was essentially hierarchical [fig. 1.4 in Howard and Reed (Howard and Reed, 1998)]. Briefly, one metathoracic femur from each locust was randomly selected for light microscopy analysis, where 12 parallel, transverse and equidistant $1 \mu\text{m}$ thick sections were cut proximally to distally using 8 mm glass knives and an ultramicrotome (EM UC6, Leica Microsystems, Wetzlar, Germany). The sections were placed onto glass slides, stained with Toluidine Blue, rinsed with distilled water and air dried. Each section was viewed between $\times 4$ and $\times 20$ magnification under an optical microscope (BX51, Olympus, Hamburg, Germany) and photographed with a mounted digital colour camera (ColorView III, Soft Imaging System, Olympus) that generated 24 bit, 2576×1932 pixel resolution images. Each section image was imported into a computer graphics program (CorelDRAW 11, Corel Corp., Ottawa, ON, Canada) where a point grid test system was superimposed randomly over the image, which allowed transverse area and volume estimates using the following stereological equations (Cruz-Orive and Weibel, 1990; Howard and Reed, 1998; Mayhew, 1991).

Femur transverse area

The number of points that fell over the femur was counted and the transverse area (T ; μm^2) was estimated for each section along the leg using:

$$T = P(a/p), \quad (1)$$

where P is the number of points falling over the femur per transverse section, and a/p is the area (μm^2) associated with each point in the grid. A mean transverse area was calculated for each section along the leg for each of the three life stages. A mean transverse area distribution curve was then generated proximally to distally along the femur for each life stage.

Femur volume

The number of points falling on muscle tissue, connective tissue, exoskeleton, class IV tracheae and air sacs (tracheae with a diameter $>20 \mu\text{m}$), tendon, nerve and haemolymph were also counted. The total volume (V ; μm^3) of each structure was then estimated for both metathoracic femurs in each locust according to the Cavalieri principle:

$$V = 2DP(a/p), \quad (2)$$

where D is the distance (μm) between sections, P is the total number of points falling on the structure summed from all 12 section images in each locust, and 2 provides a volume estimate for both metathoracic femurs per locust.

Electron microscopy

While one metathoracic femur was randomly selected for light microscopy and Cavalieri volume calculation, the remaining femur was used for transmission electron microscopy analysis. The sampling scheme used for electron microscopy randomised section position and angle to produce vertical uniform random sections (Howard and Reed, 1998; Mayhew, 1991). Six equidistant 70 nm sections were cut proximally to distally along the leg using a diamond knife (Diatome, Biel, Switzerland) and ultramicrotome. For the first locust of each life stage, the first section was cut at a random angle between 0 and 18 deg relative to the vertical plane. For the second locust, the first section was cut at a random angle between 36 and 54 deg, and for the third locust, the first section was cut at a random angle between 72 and 90 deg. For the remaining five sections in each locust, 18 deg

Table 1. Number (and magnification) of random electron micrographs taken along the length of the femur per locust

Life stage	Low-magnification femur tissue images	High-magnification muscle cell images	Trachea images	Mitochondria images
First instars ($N=3$)	40 ($\times 1950$)	40 ($\times 7900$)	40 ($\times 620-64,000$)	23 ($\times 64,000$)
Third instars ($N=3$)	41 ($\times 1950$)	41 ($\times 7900$)	41 ($\times 620-64,000$)	22 ($\times 64,000$)
Fifth instars ($N=3$)	44 ($\times 1100$)	44 ($\times 4600$)	44 ($\times 620-64,000$)	22 ($\times 64,000$)

was added to the cutting angle with every successive section. This meant that for each locust femur, the full range of angles around the vertical plane was randomly sampled.

Sections were placed onto 3 mm copper mesh grids, stained with lead citrate and viewed with a transmission electron microscope (CM 100, Philips, Eindhoven, The Netherlands), where random 8 bit, 1280×1024 pixel resolution images were captured with a mounted digital camera (MegaView II, Soft Imaging System, Olympus) at appropriate magnifications (Table 1). To obtain unbiased sampling of the femur, it was necessary to weight the number of random images taken from different sections along the leg because the femur tapers significantly as it approaches the tibial joint. The mean transverse area distribution curve generated in Eqn 1 for each life stage was used to determine the extent that sampling should be weighted towards the larger proximal regions of the leg. Accordingly, the number of random images taken from each section along the femur was adjusted as a fraction of the total number of images taken per femur (Table 1). All images were exported to CorelDRAW for analyses, where a test system was randomly superimposed over the image, which allowed estimates to be made of volume density, surface area density and thickness using the following stereological equations (Cruz-Orive and Weibel, 1990; Howard and Reed, 1998; Mayhew, 1991) appropriate for vertical sections (Baddeley et al., 1986). The average time to process each locust from initial fixation to the final quantification of femur ultrastructure was ~6 weeks. This significant investment in time restricted the study to nine individuals from three developmental stages.

Volume calculations

Low-magnification images of random femur tissue (Table 1) were analysed with a point grid test system that was randomly superimposed over the image. The total number of points falling on muscle, muscle nuclei, extracellular haemolymph, secretory cells, nerve, tendon, lipid droplets, unidentified cells and tracheae was counted. Whether points fell on tracheal lumen, cuticle, epidermis or nuclei was noted, and whether tracheae were intracellular or extracellular was also recorded. Tracheae were categorised into four size classes based on their inner diameter: class I, 0–2 μm (hereafter referred to as tracheoles); class II, 2–5 μm ; class III, 5–20 μm ; and class IV and air sacs, >20 μm [consistent with Hartung et al. (Hartung et al., 2004)]. The total volume of each structure ($V_{\text{structure}}$; μm^3) (except class IV tracheae, which was calculated in Eqn 2) within both metathoracic femurs of each locust was calculated as:

$$V_{\text{structure}} = \bar{V}_{\text{structure}} V_{\text{muscle,tissue}}, \quad (3)$$

where $\bar{V}_{\text{structure}}$ is the fraction of muscle tissue occupied by the structure determined from point grid counts, and $V_{\text{muscle,tissue}}$ is the muscle tissue volume (μm^3) of both metathoracic femurs in each locust calculated in Eqn 2.

High-magnification images of random muscle cells (Table 1) were then analysed. A point grid test system was randomly superimposed over the muscle cell image and the number of points falling on mitochondria organelles, myofibril + sarcoplasmic reticulum organelles, and cytosol was counted. Their respective volumes

($V_{\text{organelle}}$; μm^3) within both metathoracic femurs of each locust were calculated as:

$$V_{\text{organelle}} = \bar{V}_{\text{organelle}} V_{\text{muscle}}, \quad (4)$$

where $\bar{V}_{\text{organelle}}$ is the fraction of muscle cell occupied by the organelle or cytosol in each locust determined from point grid counts, and V_{muscle} is the muscle volume (μm^3) of both metathoracic femurs in each locust calculated in Eqn 3.

Mitochondrial inner membrane surface area

Mitochondria images (Table 1) were analysed using a cycloid arc test system (Fig. 2F) that was randomly translated onto the image with the minor axis of the cycloid arc parallel with the vertical direction of the image (Baddeley et al., 1986). The surface area-to-volume ratio of the inner mitochondrial membrane (SV_{inner} ; μm^{-1}) for each mitochondrion in each locust was calculated as:

$$SV_{\text{inner}} = 2I / L, \quad (5)$$

where I is the number of intersections of the test lines with the inner mitochondrial membrane surface, L is the total length (μm) of test lines falling over the mitochondrion, and 2 is the coefficient used to transform intersection points to a surface area estimate.

The total surface area of inner mitochondrial membrane (S_{inner} ; μm^2) within both femurs of each locust was calculated as:

$$S_{\text{inner}} = SV_{\text{inner}} V_{\text{mito}}, \quad (6)$$

where V_{mito} is the volume (μm^3) of mitochondria in both femurs of each locust calculated in Eqn 4.

Tracheal surface areas

Trachea images (Table 1) were analysed using a cycloid arc test system (Fig. 2F) randomly translated over the image with the minor axis of the cycloid arc parallel with the vertical direction of the image (Baddeley et al., 1986). The ratios of tracheal inner cuticle surface area-to-lumen volume (SV_{cut} ; μm^{-1}) and tracheal outer epidermal surface area-to-lumen+cuticle+epidermal volume (SV_{epi} ; μm^{-1}) (Fig. 1) for each trachea in each locust were calculated as:

$$SV_{\text{cut}} = 2I_{\text{cut}} / L_{\text{lum}}, \quad (7)$$

$$SV_{\text{epi}} = 2I_{\text{epi}} / L_{\text{lum+cut+epi}}, \quad (8)$$

where I_{cut} and I_{epi} are the number of intersections of the test lines with the inner cuticle surface and outer epidermal surface, respectively, L_{lum} and $L_{\text{lum+cut+epi}}$ are the total length (μm) of test lines falling over the tracheal lumen and tracheal lumen + cuticle + epidermis, respectively, and 2 is the coefficient used to transform intersection points to a surface area estimate.

The total surface area of the inner cuticle layer (S_{cut} ; μm^2) and outer epidermal layer (S_{epi} ; μm^2) (Fig. 1) for each trachea size class (I, II, III and IV) within both femurs of each locust was calculated as:

$$S_{\text{cut}} = SV_{\text{cut}} V_{\text{trach,lum}}, \quad (9)$$

$$S_{\text{epi}} = SV_{\text{epi}} V_{\text{trach,lum+cut+epi}}, \quad (10)$$

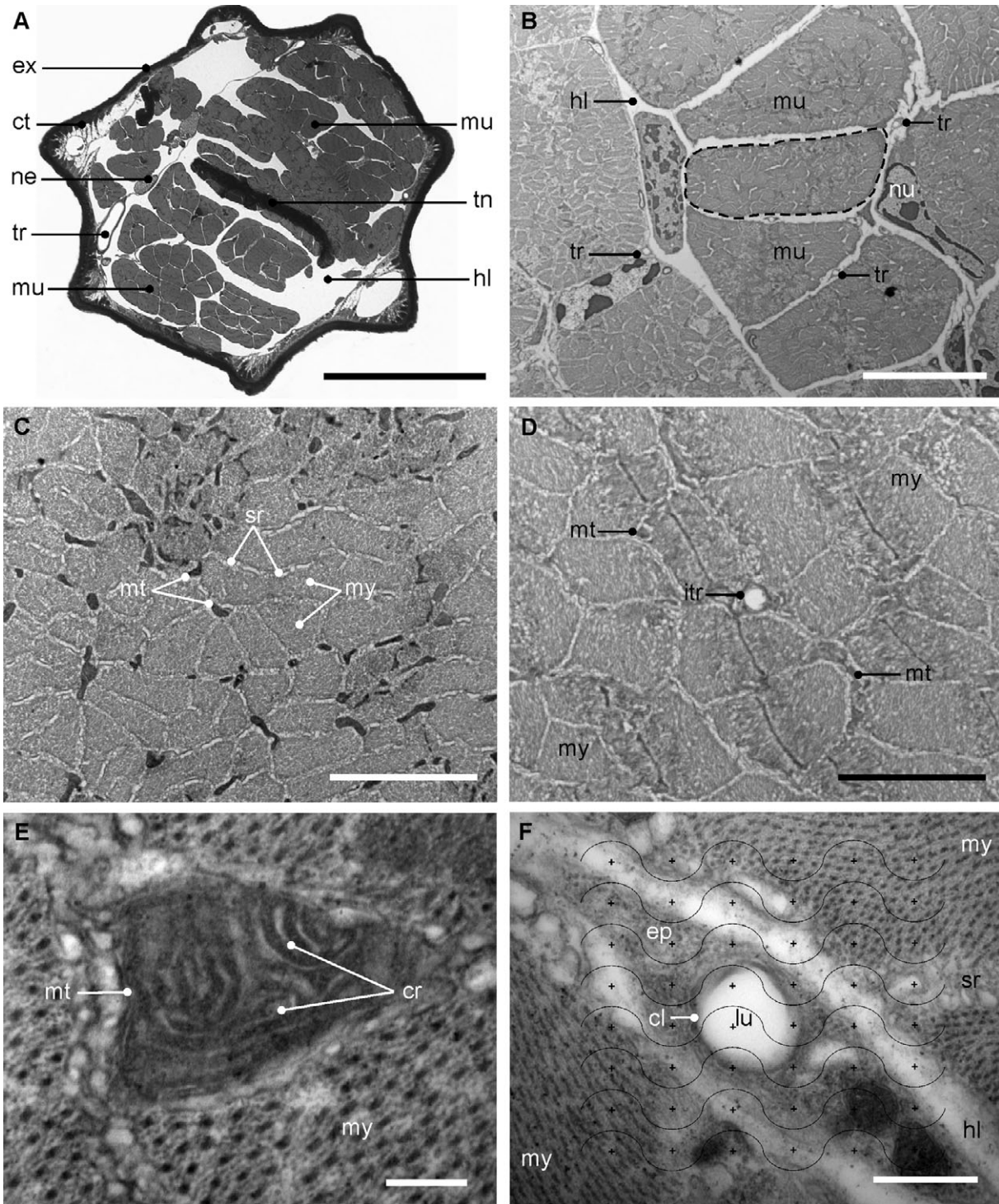


Fig. 2. Micrographs from the locust metathoracic femur showing the hierarchy of magnifications used to quantify every structure referred to in the Materials and methods (see Table 1 for electron micrograph magnifications). (A) An example of a low magnification light micrograph from which the volume of muscle tissue (and other tissue types) was calculated according to the Cavalieri principle. First instar; scale bar, 200 μm . (B) Low-magnification electron micrograph from which the volume fraction of muscle tissue occupied by muscle cells (a single muscle cell is indicated by the dashed outline in the image), tracheae, and other structures was calculated. First instar; scale bar, 10 μm . (C,D) High-magnification electron micrographs of the ultra-structure of a random muscle cell from which the volume fraction occupied by mitochondria and myofibril + sarcoplasmic reticulum organelles was calculated. Fifth instar; scale bar, 5 μm . (E) Very high magnification electron micrograph of a random mitochondrion from which the surface area-to-volume ratio of the inner membrane was calculated. First instar; scale bar, 0.2 μm . (F) Very high magnification electron micrograph of a random class I trachea (tracheole) with a randomly translated cycloid arc test system superimposed over the image, which was used to calculate the surface area-to-volume ratio of the cuticular and epidermal layers, and as the starting point in the thickness measurements of the respective layers. First instar; scale bar, 0.5 μm . Abbreviations: cl, cuticle layer; cr, mitochondrial cristae; ct, connective tissue; ep, epidermal layer; ex, exoskeleton; hl, haemolymph; itr, intracellular tracheole; lu, lumen; mt, mitochondrion; mu, muscle; my, myofibril; ne, nerve; nu, nucleus; sr, sarcoplasmic reticulum; tn, tendon; tr, trachea.

where $S_{V_{cut}}$ and $S_{V_{epi}}$ are the mean tracheal inner cuticle surface area-to-lumen volume ratio and mean tracheal outer epidermal surface area-to-lumen + cuticle + epidermis volume ratio (μm^{-1}), respectively, which were calculated for each trachea size class for each locust in Eqns 7 and 8, respectively. $V_{trach,lum}$ and $V_{trach,lum+cut+epi}$ are the volumes (μm^3) of the lumen and the lumen + cuticle + epidermis in both femurs of each locust, respectively, both of which were calculated in Eqn 3 for class I, II and III tracheae, and in Eqn 2 for class IV tracheae.

Tracheal thickness measurements

Trachea images (Table 1) were reanalysed, this time to determine the thickness of both the cuticular and epidermal layers (Fig. 1). Four random intersections made by the superimposed cycloid arc test system (Fig. 2F) with the inner cuticular layer were used as the starting point of the measurement, from which the thickness of the inner cuticle and the outer epidermal layers were measured in a random direction [consistent with other tracheal morphometry studies (Hartung et al., 2004; Schmitz and Perry, 2001)]. The harmonic mean barrier thickness of the cuticular (τ_{cut} ; μm) and epidermal (τ_{epi} ; μm) layers for each trachea size class (I, II, III and IV) in each locust was calculated as:

$$\tau = (N / \sum_{i=1}^N \frac{1}{L_i})^{2/3}, \quad (11)$$

where N is the number of measurements, L_i are the individual measured lengths (μm), and $2/3$ compensates for an overestimation due to the random orientation of measured intercepts (Weibel and Knight, 1964).

Lateral diffusing capacity

The lateral diffusing capacity for oxygen (i.e. lateral conductance; $\mu\text{mol O}_2 \text{kPa}^{-1} \text{h}^{-1}$) was determined separately for the cuticle layer ($G_{L,cut}$) and epidermal layer ($G_{L,epi}$) (Fig. 1) of each trachea size class (I, II, III and IV) for both femurs of each locust. It was calculated as:

$$G_{L,cut} = S_{cut} / \tau_{cut} K_{cut}, \quad (12)$$

$$G_{L,epi} = S_{cut} / \tau_{epi} K_{epi}, \quad (13)$$

where S_{cut} is the tracheal inner cuticle surface area (μm^2) for each trachea size class for both femurs of each locust calculated in Eqn 9, τ_{cut} and τ_{epi} are the harmonic mean barrier thicknesses (μm) of the cuticle and epidermal layers, respectively, for each trachea size class in each locust calculated in Eqn 11, and K_{cut} and K_{epi} are the Krogh diffusion coefficients for chitin ($3.95 \times 10^{-9} \mu\text{mol O}_2 \text{kPa}^{-1} \text{h}^{-1} \mu\text{m}^{-1}$) and rat lung tissue ($6.31 \times 10^{-8} \mu\text{mol O}_2 \text{kPa}^{-1} \text{h}^{-1} \mu\text{m}^{-1}$), respectively, corrected to 35°C using $Q_{10}=1.1$ (Bartels, 1971), consistent with the temperature of respirometry experiments (Snelling et al., 2011).

The lateral diffusing capacity ($G_{L,trach}$; $\mu\text{mol O}_2 \text{kPa}^{-1} \text{h}^{-1}$) of each trachea size class (I, II, III and IV) within both femurs of each locust was calculated as:

$$G_{L,trach} = 1 / (1 / G_{L,cut} + 1 / G_{L,epi}). \quad (14)$$

This is appropriate for determining overall conductance in series (Weibel, 1970).

The lateral diffusing capacity of the entire tracheal system ($G_{L,trach,sys}$; $\mu\text{mol O}_2 \text{kPa}^{-1} \text{h}^{-1}$) within both femurs of each locust was calculated as:

$$G_{L,trach,sys} = G_{L,trachI} + G_{L,trachII} + G_{L,trachIII} + G_{L,trachIV}, \quad (15)$$

where $G_{L,trachI}$, $G_{L,trachII}$, $G_{L,trachIII}$ and $G_{L,trachIV}$ are the lateral diffusing capacities ($\mu\text{mol O}_2 \text{kPa}^{-1} \text{h}^{-1}$) of each trachea size class within both femurs of each locust calculated in Eqn 14.

Radial diffusing capacity

The radial diffusing capacity for oxygen (i.e. radial conductance) out of the class I tracheae (tracheoles) and into the surrounding muscle was calculated for each locust according to Krogh's cylinder model for radial diffusion (Kreuzer, 1982; Krogh, 1919). Krogh's cylinder (Fig. 1) was adapted only for tracheoles because they are the most relevant in the supply of oxygen to the tissues (see Results).

Images of tracheoles were reanalysed and the inner cuticular radius (r_{cut} ; μm) was measured and averaged for each locust. According to Krogh's model, the tracheoles and the surrounding muscle they service are cylindrical in shape. Therefore, the mean radius (μm) to the outer surface of the cuticle layer (R_{cut}), epidermal layer (R_{epi}) and serviced muscle (R_{muscle}) can be calculated for each locust according to:

$$R_{cut} = r_{cut} + \tau_{cut}, \quad (16)$$

$$R_{epi} = R_{cut} + \tau_{epi}, \quad (17)$$

$$R_{muscle} = \sqrt{r_{cut}^2 (T_{muscle} / T_{lumi})}, \quad (18)$$

where τ_{cut} and τ_{epi} are the harmonic mean barrier thicknesses (μm) of the cuticular and epidermal layers of the tracheoles, respectively, calculated for each locust in Eqn 11, and T_{muscle}/T_{lumi} is the ratio between the mean transverse area of muscle that surrounds each tracheole and the mean transverse area of the tracheole lumen. This is equal to the ratio between the volume of muscle and the volume of tracheole lumen, which were quantified for each locust in Eqn 3.

The radial diffusing capacity ($\mu\text{mol O}_2 \text{kPa}^{-1} \text{h}^{-1}$) of the inner cuticle layer of the tracheoles ($G_{R,cut}$), the outer epidermal layer of the tracheoles ($G_{R,epi}$), and the muscle that surrounds the tracheoles ($G_{R,muscle}$) within both femurs for each locust was calculated according to Krogh's cylinder model for radial diffusion (Fig. 1) [adapted from Kreuzer (Kreuzer, 1982)]:

$$G_{R,cut} = K_{cut} / \left[\frac{R_{cut}^2}{2} \ln \frac{R_{cut}}{r_{cut}} - \frac{R_{cut}^2 - r_{cut}^2}{4} \right] V_{cut}, \quad (19)$$

$$G_{R,epi} = K_{epi} / \left[\frac{R_{epi}^2}{2} \ln \frac{R_{epi}}{r_{cut}} - \frac{R_{epi}^2 - r_{cut}^2}{4} \right] V_{epi}, \quad (20)$$

$$G_{R,muscle} = K_{muscle} / \left[\frac{R_{muscle}^2}{2} \ln \frac{R_{muscle}}{r_{cut}} - \frac{R_{muscle}^2 - r_{cut}^2}{4} \right] V_{muscle}, \quad (21)$$

where V_{cut} , V_{epi} and V_{muscle} are the tracheole cuticle, tracheole epidermal and muscle volumes (μm^3) in both femurs, respectively, calculated for each locust in Eqn 3. K_{cut} , K_{epi} and K_{muscle} are the Krogh diffusion coefficients for chitin, rat lung tissue and frog muscle ($4.16 \times 10^{-8} \mu\text{mol O}_2 \text{kPa}^{-1} \text{h}^{-1} \mu\text{m}^{-1}$), respectively, corrected to 35°C using $Q_{10}=1.1$ (Bartels, 1971).

Finally, the total radial diffusing capacity for oxygen across the cuticular and epidermal layers of the tracheoles and through the surrounding muscle serviced by the tracheoles ($G_{R,trachI}$; $\mu\text{mol O}_2 \text{kPa}^{-1} \text{h}^{-1}$) in both femurs for each locust was calculated as:

$$G_{R,trachI} = 1 / (1 / G_{R,cut} + 1 / G_{R,epi} + 1 / G_{R,muscle}). \quad (22)$$

All mean values and allometric exponents include $\pm 95\%$ confidence intervals (CI), unless otherwise stated. Allometric data were \log_{10} -transformed before statistical analysis using ordinary least-squares

regressions. Analysis of covariance (ANCOVA) comparisons of regressions (Zar, 1998) were carried out with GraphPad Prism 5.

RESULTS

Body mass

Body mass increased 32-fold throughout juvenile development. First instars had a mean wet body mass of 0.019 ± 0.001 g ($N=3$), which increased to 0.122 ± 0.007 g by the third instar stage ($N=3$) and 0.611 ± 0.010 g by the fifth instar stage ($N=3$). There was no significant difference between the body mass of locusts used in the present study and those used in earlier respirometry experiments (Snelling et al., 2011) for each life stage (Mann–Whitney U -test, $P > 0.05$).

Allometric variation

Muscle volume

Muscle occupies approximately half the volume of the metathoracic femur (Fig. 2A,B), and muscle volume scales according to the allometric power equation $V_{\text{muscle}} = 4.3 \times 10^{10} M_b^{1.05 \pm 0.08} \mu\text{m}^3$ ($r^2 = 0.99$, $N=9$; Fig. 3B; supplementary material Table S1). Earlier respirometry experiments (Snelling et al., 2011) found that the maximum functional rate at which oxygen is consumed by jumping muscle during intense hopping exercise scales according to the equation $\dot{M}M_{\text{O}_2, \text{juv, hop}} = 103 M_b^{1.02 \pm 0.02} \mu\text{mol O}_2 \text{h}^{-1}$ at 35°C ($r^2 = 0.98$, $N=145$). The exponent for $\dot{M}M_{\text{O}_2, \text{juv, hop}}$ is not significantly different to V_{muscle} (ANCOVA, $F_{1,150} = 0.43$, $P = 0.51$).

Mitochondrial volume

Mitochondria occupy approximately 3.5% of muscle cell volume regardless of life stage (Fig. 2C,D; Table 2). This is indicated in the allometric power equation for mitochondrial volume density, $V_{\text{mito}} = 0.032 M_b^{-0.03 \pm 0.09} \mu\text{m}^3$ ($r^2 = 0.10$, $N=9$; supplementary material Table S2).

The absolute volume of mitochondria in the hopping muscle is highly dependent on body mass and scales according to the equation $V_{\text{mito}} = 1.3 \times 10^9 M_b^{1.02 \pm 0.08} \mu\text{m}^3$ ($r^2 = 0.99$, $N=9$; Fig. 3C; supplementary material Table S3). The exponent for V_{mito} is not significantly different to $\dot{M}M_{\text{O}_2, \text{juv, hop}}$ (ANCOVA, $F_{1,150} = 0.01$, $P = 0.94$).

Mitochondrial inner membrane surface area

The surface density of inner membrane within the mitochondria is similar for all life stages and averages approximately $33 \mu\text{m}^2 \mu\text{m}^{-3}$ (Fig. 2E; Table 2). Inner mitochondrial membrane surface density scales according to the allometric power equation $S_{\text{inner}} = 31 M_b^{-0.03 \pm 0.05} \mu\text{m}^{-1}$ ($r^2 = 0.23$, $N=9$; supplementary material Table S4).

The total surface area of inner mitochondrial membrane in the hopping muscle is highly dependent on body mass and scales according to the equation $S_{\text{inner}} = 4.2 \times 10^{10} M_b^{0.99 \pm 0.10} \mu\text{m}^2$ ($r^2 = 0.99$, $N=9$; Fig. 3D). The exponent for S_{inner} is not significantly different to $\dot{M}M_{\text{O}_2, \text{juv, hop}}$ (ANCOVA, $F_{1,150} = 0.52$, $P = 0.47$).

Tracheal volume

The tracheal system occupies approximately 3% of the metathoracic femur volume. The volume of the tracheal system within both metathoracic femurs scales hypermetrically with body mass following the allometric power equation $V_{\text{trach, sys}} = 2.4 \times 10^9 M_b^{1.12 \pm 0.09} \mu\text{m}^3$ ($r^2 = 0.99$, $N=9$; Fig. 3E; supplementary material Table S5), which has an exponent that is significantly greater than the exponent derived for $\dot{M}M_{\text{O}_2, \text{juv, hop}}$ (ANCOVA, $F_{1,150} = 4.44$, $P < 0.05$).

However, class IV tracheae and air sacs account for much of the tracheal system's volume: 68% in first instars, 71% in third

instars and 78% in fifth instars (Table 3). The volume of class IV tracheae and air sacs increase disproportionately with body mass according to the power equation $V_{\text{trachIV}} = 1.9 \times 10^9 M_b^{1.16 \pm 0.16} \mu\text{m}^3$ ($r^2 = 0.98$, $N=9$). If class IV tracheae and air sacs are excluded, then the volume of the tracheal system scales with a much lower exponent following the equation $V_{\text{trach, sys-trachIV}} = 5.4 \times 10^8 M_b^{1.02 \pm 0.14} \mu\text{m}^3$ ($r^2 = 0.98$, $N=9$), which has an exponent that is statistically indistinguishable from that derived for $\dot{M}M_{\text{O}_2, \text{juv, hop}}$ (ANCOVA, $F_{1,150} = 0.00$, $P = 0.97$).

Class II and III tracheae are relatively uncommon, representing just 5–10% of the tracheal system's volume despite their reasonably large size (Table 3).

Class I tracheae (tracheoles) contribute 10–15% of the tracheal system's volume (Table 3) and, because of their small size, are far more numerous than the other trachea size classes (Fig. 2B,D,F). The volume density of tracheoles in the muscle is largely invariant with body mass and scales according to the allometric equation $V_{\text{trachI}} = 0.0073 M_b^{0.06 \pm 0.24} \mu\text{m}^3$ ($r^2 = 0.04$, $N=9$). The volume density of tracheole lumen in the muscle scales according to the equation $V_{\text{trachI, lum}} = 0.00051 M_b^{-0.06 \pm 0.15} \mu\text{m}^3$ ($r^2 = 0.12$, $N=9$). However, the absolute volume of tracheoles in the femurs is highly dependent on body mass and scales according to the equation $V_{\text{trachI}} = 3.1 \times 10^8 M_b^{1.11 \pm 0.23} \mu\text{m}^3$ ($r^2 = 0.95$, $N=9$; Fig. 3F). The absolute volume of tracheole lumen in the femurs is less, and scales according to the equation $V_{\text{trachI, lum}} = 2.2 \times 10^7 M_b^{0.99 \pm 0.16} \mu\text{m}^3$ ($r^2 = 0.97$, $N=9$; Fig. 3G). Neither the exponent for V_{trachI} (ANCOVA, $F_{1,150} = 2.87$, $P = 0.09$) nor that for $V_{\text{trachI, lum}}$ (ANCOVA, $F_{1,150} = 0.35$, $P = 0.56$) are significantly different to $\dot{M}M_{\text{O}_2, \text{juv, hop}}$.

Tracheal surface area

The area of the tracheal system's outer epidermal surface in both femurs scales according to the allometric power equation $S_{\text{epi, trach, sys}} = 1.8 \times 10^9 M_b^{1.10 \pm 0.17} \mu\text{m}^2$ ($r^2 = 0.97$, $N=9$; supplementary material Table S5). The class I trachea (tracheole) outer epidermal surface area scales with juvenile body mass following the equation $S_{\text{epiI}} = 1.5 \times 10^9 M_b^{1.11 \pm 0.23} \mu\text{m}^2$ ($r^2 = 0.95$, $N=9$), which is not significantly different to the exponent derived for $\dot{M}M_{\text{O}_2, \text{juv, hop}}$ (ANCOVA, $F_{1,150} = 2.87$, $P = 0.09$).

The area of the tracheal system's inner cuticular surface in both femurs scales according to the allometric equation, $S_{\text{cut, trach, sys}} = 8.5 \times 10^8 M_b^{1.16 \pm 0.43} \mu\text{m}^2$ ($r^2 = 0.85$, $N=9$). The tracheole inner cuticle surface area scales with body mass following the equation $S_{\text{cutI}} = 2.0 \times 10^8 M_b^{0.99 \pm 0.16} \mu\text{m}^2$ ($r^2 = 0.97$, $N=9$; Fig. 3H), which is similar to the exponent derived for $\dot{M}M_{\text{O}_2, \text{juv, hop}}$ (ANCOVA, $F_{1,150} = 0.35$, $P = 0.56$).

Tracheal harmonic mean barrier thickness

The harmonic mean barrier thickness of the cuticular and epidermal layers increases with trachea size class (supplementary material Table S5). Class I tracheae (tracheoles) thus have the thinnest walls. The harmonic mean barrier thickness of the tracheole cuticle and epidermal layers does not vary with body mass. Tracheole harmonic mean barrier cuticle thickness scales according to the allometric equation $\tau_{\text{cutI}} = 0.027 M_b^{-0.01 \pm 0.05} \mu\text{m}$ ($r^2 = 0.05$, $N=9$), and the harmonic mean barrier epidermal thickness scales according to the equation $\tau_{\text{epiI}} = 0.19 M_b^{0.04 \pm 0.17} \mu\text{m}$ ($r^2 = 0.04$, $N=9$).

Tracheal lateral diffusing capacity

The lateral diffusing capacity (lateral conductance) of the entire tracheal system in the femurs scales isometrically with body mass following the equation $G_{\text{L, trach, sys}} = 23 M_b^{1.00 \pm 0.21} \mu\text{mol O}_2 \text{kPa}^{-1} \text{h}^{-1}$ at

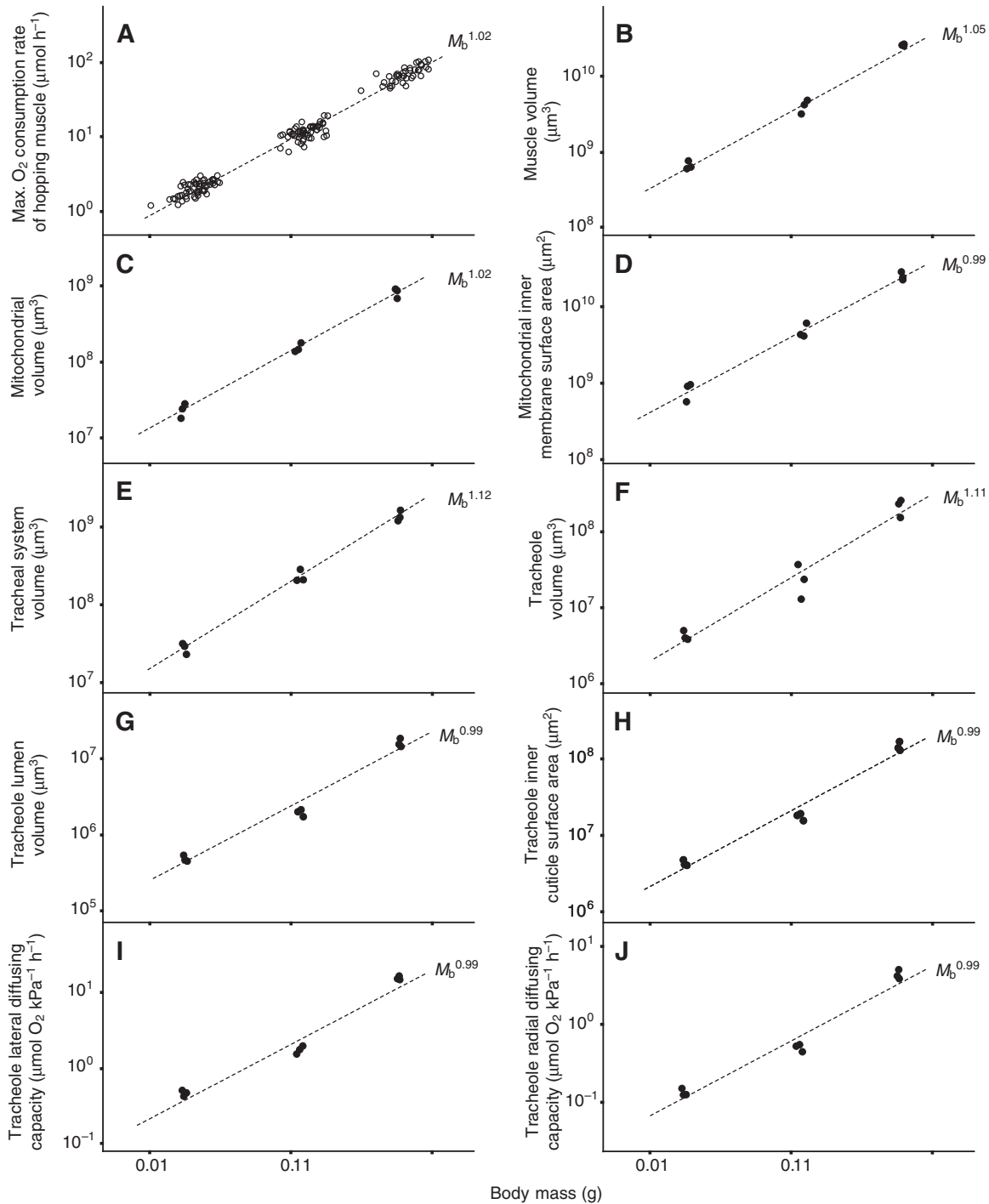


Fig. 3. Relationship between body mass and (A) maximum oxygen consumption rate of juvenile hopping muscle, $\dot{M}_{M_{O_2,juv,hop}}$, during intense jumping exercise in first ($N=55$), third ($N=53$) and fifth instar locusts ($N=37$); (B) muscle volume; (C) mitochondrial volume; (D) mitochondrial inner membrane surface area; (E) total tracheal system volume; (F) class I tracheal (tracheole) volume; (G) tracheole lumen volume; (H) tracheole inner cuticle surface area; (I) tracheole lateral diffusing capacity; and (J) tracheole radial diffusing capacity. Data shown in B–J are for both metathoracic femurs in first ($N=3$), third ($N=3$) and fifth instar locusts ($N=3$).

35°C ($r^2=0.95$, $N=9$; supplementary material Table S6), which is not significantly different to the exponent derived for $\dot{M}_{M_{O_2,juv,hop}}$ (ANCOVA, $F_{1,150}=0.21$, $P=0.64$).

Class I tracheae (tracheoles) provide ~90% of the lateral diffusing capacity of the entire tracheal system in the femurs (Table 4). The lateral diffusing capacity of tracheoles scales according to the allometric equation $G_{L,trachi}=20M_b^{0.99\pm 0.17} \mu\text{mol O}_2 \text{ kPa}^{-1} \text{ h}^{-1}$ at 35°C

($r^2=0.96$, $N=9$; Fig. 3I), which is also not significantly different to the exponent derived for $\dot{M}_{M_{O_2,juv,hop}}$ (ANCOVA, $F_{1,150}=0.40$, $P=0.53$).

Tracheole radial diffusing capacity

The mean transverse area of muscle serviced by each tracheole is $440 \mu\text{m}^2$ (radius = $12 \mu\text{m}$) and scales independently with body mass

Table 2. Volume of hopping muscle, myofibril + sarcoplasmic reticulum, and mitochondria within both metathoracic femurs in first ($N=3$), third ($N=3$) and fifth instar locusts ($N=3$)

	First instars	Third instars	Fifth instars
Muscle volume of femur (μm^3)	$6.8 \times 10^8 \pm 9.6 \times 10^7$	$4.2 \times 10^9 \pm 9.7 \times 10^8$	$2.7 \times 10^{10} \pm 7.7 \times 10^8$
Myofibril + sarcoplasmic reticulum volume in muscle (μm^3)	$6.3 \times 10^8 \pm 9.3 \times 10^7$	$3.9 \times 10^9 \pm 9.1 \times 10^8$	$2.5 \times 10^{10} \pm 6.2 \times 10^8$
Mitochondrial volume in muscle (μm^3)	$2.4 \times 10^7 \pm 5.7 \times 10^6$	$1.6 \times 10^8 \pm 2.4 \times 10^7$	$8.3 \times 10^8 \pm 1.3 \times 10^8$
Myofibril + sarcoplasmic reticulum density in muscle (%)	92.8±1.7	92.5±0.9	94.4±0.6
Mitochondrial density in muscle (%)	3.5±0.9	3.8±0.5	3.1±0.4
Mitochondrial inner membrane surface area (μm^2)	$8.5 \times 10^8 \pm 2.4 \times 10^8$	$5.1 \times 10^9 \pm 1.3 \times 10^9$	$2.6 \times 10^{10} \pm 3.9 \times 10^9$
Mitochondrial inner membrane surface density (μm^{-1})	35.5±3.7	32.4±3.4	32.0±3.3

Also shown is the volume density of myofibril + sarcoplasmic reticulum and mitochondria in the hopping muscle, and the mitochondrial inner membrane surface area and surface density.

Data are means \pm 95% CI.

according to the allometric relationship $T_{\text{muscle}} = 482M_b^{0.06 \pm 0.15} \mu\text{m}^2$ ($r^2=0.12$, $N=9$).

The radial diffusing capacity (radial conductance) for oxygen through the tracheole cuticle, epidermis and surrounding muscle scales with juvenile body mass according to the allometric equation $G_{R,\text{trachi}} = 5.8M_b^{0.99 \pm 0.18} \mu\text{mol O}_2 \text{kPa}^{-1} \text{h}^{-1}$ at 35°C ($r^2=0.96$, $N=9$; Fig. 3J; supplementary material Table S6), which is statistically similar to the exponent derived for $\dot{M}_{\text{M}_{\text{O}_2, \text{juv, hop}}}$ (ANCOVA, $F_{1,150}=0.55$, $P=0.46$).

DISCUSSION

Respirometry conducted prior to the present study revealed that the maximum functional rate at which oxygen is delivered and consumed by the juvenile hopping muscle during strenuous jumping exercise, $\dot{M}_{\text{M}_{\text{O}_2, \text{juv, hop}}}$, scales with body mass with an exponent of 1.02 ± 0.02 (Snelling et al., 2011). According to the principles of symmorphosis, the structures involved in the delivery (tracheal system) and consumption (mitochondria) of oxygen should scale congruently with maximum oxygen consumption rate (Weibel et al., 1991).

Mitochondria as oxygen sinks

The volume of hopping muscle contained within the metathoracic femurs (Fig. 2A,B) scales with an exponent of 1.05 (Fig. 3B). Contained within the muscle fibres are mitochondria (Fig. 2C,D) that occupy approximately 3.5% of muscle volume in all locusts (Table 2), which agrees well with the results of another study that estimated a mitochondrial density of approximately 2–4% in the hopping muscle of American locusts, *Schistocerca americana*

(Hartung et al., 2004). However, it is considerably less than the 20–50% mitochondrial density estimated for insect flight muscle, which is no doubt related to the much higher energetic requirements for flight compared with terrestrial locomotion (Mizisin and Ready, 1986; Smith, 1963).

The volume of mitochondria in the hopping muscle scales with an exponent of 1.02 (Fig. 3C) and is parallel with the scaling of the hopping muscle's aerobic capacity. The congruent scaling of structure and function suggests that no more mitochondria exist than are necessary to meet the maximum energy requirements of the exercising muscle, which is indicative of symmorphosis. Matching at this step of the oxygen cascade has also been shown in the locomotory and diaphragm muscles of mammals (Mathieu et al., 1981; Schwerzmann et al., 1989; Weibel et al., 2004).

Within the mitochondria, the respiratory enzymes for oxidative phosphorylation are located in the inner membrane (Fig. 2E), and so it is reasonable to argue that quantifying the inner membrane surface area is a more relevant test for symmorphosis. Mitochondria in locust hopping muscle have a mean inner membrane surface density of approximately $33 \mu\text{m}^2 \mu\text{m}^{-3}$ (Table 2). This is similar to cat muscle mitochondria, which have an inner membrane surface density of approximately $35 \mu\text{m}^2 \mu\text{m}^{-3}$ (Schwerzmann et al., 1989), but is much less than the flight muscle of flies (Smith, 1963) and hummingbirds (Suarez et al., 1991), which are in the vicinity of $50\text{--}60 \mu\text{m}^2 \mu\text{m}^{-3}$. It is speculated that in these animals, the inner membrane surface density is at the upper limit, beyond which there would be insufficient room in the mitochondrial matrix for Krebs cycle enzymes to function properly (Suarez, 1996).

 Table 3. Class I tracheal (tracheole) inner cuticle and outer epidermal surface area, class I tracheal volume density, class I, II, III and IV tracheal volume, and the total tracheal system volume within both metathoracic femurs in first ($N=3$), third ($N=3$) and fifth instar locusts ($N=3$)

	First instars	Third instars	Fifth instars
Class I tracheal inner cuticle surface area (μm^2)	$4.4 \times 10^6 \pm 4.7 \times 10^5$	$1.8 \times 10^7 \pm 2.1 \times 10^6$	$1.5 \times 10^8 \pm 2.3 \times 10^7$
Class I tracheal outer epidermal surface area (μm^2)	$2.0 \times 10^7 \pm 3.3 \times 10^6$	$1.2 \times 10^8 \pm 6.4 \times 10^7$	$1.0 \times 10^9 \pm 2.9 \times 10^8$
Class I tracheal density in muscle, lumen only (%)	0.072±0.015	0.048±0.015	0.060±0.011
Class I tracheal density in muscle (%)	0.645±0.173	0.638±0.496	0.802±0.209
Class I tracheal volume, lumen only (μm^3)	$4.8 \times 10^5 \pm 5.1 \times 10^4$	$1.9 \times 10^6 \pm 2.3 \times 10^5$	$1.6 \times 10^7 \pm 2.5 \times 10^6$
Class I tracheal volume (μm^3)	$4.3 \times 10^6 \pm 7.1 \times 10^5$	$2.5 \times 10^7 \pm 1.4 \times 10^7$	$2.2 \times 10^8 \pm 6.1 \times 10^7$
Class II tracheal volume (μm^3)	$1.2 \times 10^6 \pm 7.5 \times 10^5$	$7.4 \times 10^6 \pm 5.4 \times 10^6$	$4.0 \times 10^7 \pm 1.6 \times 10^7$
Class III tracheal volume (μm^3)	$3.5 \times 10^6 \pm 1.2 \times 10^6$	$3.8 \times 10^7 \pm 4.1 \times 10^7$	$7.0 \times 10^7 \pm 5.7 \times 10^7$
Class IV tracheal volume (μm^3)	$1.9 \times 10^7 \pm 4.3 \times 10^6$	$1.7 \times 10^8 \pm 7.7 \times 10^7$	$1.1 \times 10^9 \pm 1.6 \times 10^8$
Total tracheal volume (μm^3)	$2.8 \times 10^7 \pm 5.4 \times 10^6$	$2.4 \times 10^8 \pm 5.1 \times 10^7$	$1.4 \times 10^9 \pm 2.5 \times 10^8$

Data are means \pm 95% CI.

Table 4. Anatomical radial diffusing capacity of class I tracheae (tracheoles), and anatomical lateral diffusing capacity of class I, II, III and IV tracheae and the entire tracheal system within both metathoracic femurs in first ($N=3$), third ($N=3$) and fifth instar locusts ($N=3$)

	First instars	Third instars	Fifth instars
Class I radial conductance	0.134±0.017	0.506±0.060	4.353±0.714
Class I lateral conductance	0.461±0.044	1.712±0.229	15.144±0.896
Class II lateral conductance	0.017±0.006	0.030±0.024	0.248±0.006
Class III lateral conductance	0.010±0.006	0.037±0.019	0.125±0.040
Class IV lateral conductance	0.053±0.067	0.050±0.026	2.595±4.388
Total tracheal system lateral conductance	0.541±0.025	1.829±0.213	18.112±5.322

Data are means ± 95% CI, in units of $\mu\text{mol O}_2 \text{kPa}^{-1} \text{h}^{-1}$.

The mitochondrial inner membrane surface density in hopping muscle decreases very slightly with age (Table 2), which probably reflects the gradual increase in mitochondrion size that occurs during development rather than a decrease in the density at which cristae are packed. The absolute surface area of mitochondrial inner membrane therefore scales with an exponent of 0.99 (Fig. 3D), which is statistically similar to the exponent derived for the hopping muscle's aerobic capacity. Therefore, at this final step of the oxygen cascade, the principles of symmorphosis are evident.

Oxygen delivery and the tracheal system

The volume of the entire tracheal system within the metathoracic femur scales with an exponent of 1.12 (Fig. 3E), which is significantly greater than the scaling of the hopping muscle's maximum oxygen consumption rate. This suggests that larger locusts may have more tracheae than they require, which runs counter to the principles of economic design implicit with the symmorphosis hypothesis. However, it is worth examining each trachea size class separately because different sized tracheae may perform different functions.

More than half the tracheal volume can be attributed to large class IV tracheae and air sacs (Table 3), which scale with a rather steep exponent of 1.16. This means that large locusts have relatively more large-sized tracheae. However, the harmonic mean barrier thickness of class IV tracheae is very thick, and so although they represent more than half the total tracheal volume, they provide less than 5% of the overall lateral diffusing capacity (Table 4). The large size and poor lateral conductance of class IV tracheae suggest that their main function is to ventilate the tracheal system (Maina, 1989; Weis-Fogh, 1967; Westneat et al., 2003). If this is correct, then the disproportionately greater volume of class IV tracheae in older locusts could be necessary to overcome the physiological diffusion limitations associated with long tracheal tubes in larger insects (Greenlee et al., 2009; Harrison et al., 2005; Kaiser et al., 2007). The idea that large insects are diffusion limited is central to the hypothesis that insect gigantism during the late Palaeozoic was facilitated by hyperoxic atmospheres that occurred around the same time (Dudley, 1998; Graham et al., 1995).

Class II and III tracheae each represent just ~3% of the tracheal system's volume and total surface area in the femur (Table 3). Compared with larger class IV tracheae, their walls are thinner and so they probably allow a small amount of oxygen to diffuse across, but because they are so uncommon, they account for less than 3% of the tracheal system's overall lateral diffusing capacity (Table 4). Therefore, it seems that the primary function of class II and III tracheae is to serve as an intermediary between class IV and class I tracheae.

Small class I tracheae (tracheoles) represent the terminal endings of the tracheal system and contribute 13% to overall tracheal volume

and less than 1% to muscle volume in the femur (Table 3). Tracheole volume scales with an exponent of 1.11 (Fig. 3F), which is higher than the 1.02 derived for the hopping muscle's aerobic capacity, but the difference is not significant. However, oxygen is delivered along the tracheoles in the gas phase, and so it is more useful to analyse the lumen volume only, which excludes the cuticular and epidermal components that are important only in the across-wall diffusion of oxygen. The lumen volume of tracheoles scales with an exponent of 0.99 (Fig. 3G) and this is well matched to the aerobic capacity of the juvenile hopping muscle. Thus, although the volume of the entire tracheal system is not symmorphotic, the functional part is.

To reach the exercising muscle, oxygen must first diffuse across the tracheole inner cuticle layer followed by the outer epidermal layer. The tracheole outer epidermal layer has a surface density of approximately $4 \mu\text{m}^2 \mu\text{m}^{-3}$, and its total surface area scales with body mass with an exponent of 1.11, which is somewhat higher than the exponent derived for the hopping muscle's maximum oxygen consumption rate. However, given that the outer epidermal surface covers a greater area than the inner cuticle surface, it would seem that the inner cuticle layer is far more important in terms of limiting oxygen flow out of the tracheoles (Fig. 2F; Table 3). The tracheole inner cuticle layer has a surface density of approximately $8 \mu\text{m}^2 \mu\text{m}^{-3}$, and its total surface area scales with body mass with an exponent of 0.99 (Fig. 3H), which is congruent with the hopping muscle's aerobic capacity as predicted by symmorphosis.

The lateral diffusing capacity of the entire tracheal system within the femurs scales isometrically with body mass and approximately 90% of the system's lateral conductance for oxygen can be attributed to the tracheoles (Table 4), which are intimately associated with the muscle (Fig. 2B,D,F). Therefore, tracheoles represent the primary site for oxygen transfer from the tracheal system to the muscle, which is in agreement with the results of other morphometric studies on insects (Hartung et al., 2004; Schmitz and Perry, 1999). The harmonic mean barrier thickness of the tracheole cuticle and epidermal layers does not vary much throughout development, and so the tracheole lateral diffusing capacity scales with an exponent of 0.99 (Fig. 3I), following a slope similar to that of the inner cuticle surface area. The exponent for tracheole lateral diffusing capacity matches the scaling of the hopping muscle's maximum oxygen consumption rate, as predicted by symmorphosis.

However, the congruent scaling between lateral diffusing capacity and the hopping muscle's aerobic limits is a little surprising because the ontogenetic growth of the hopping muscle is associated with an observed increase in the size of muscle cells [also observed by Hartung et al. (Hartung et al., 2004)], which would lead to longer average diffusion distances for oxygen through the muscle. In

response to the longer diffusion distance, it is reasonable to suspect that larger locusts may have a disproportionate investment in the abundance of tracheoles as a means to compensate for this. Instead, larger locusts appear to overcome this potential diffusion problem in part by investing more in large class IV tracheae (Table 3), which function to ventilate the tracheal system and maintain a high pressure head for oxygen diffusion (Maina, 1989; Weis-Fogh, 1967; Westneat et al., 2003), and in part by increasing the number of tracheoles that penetrate the muscle cell, such that they become functionally intracellular and, therefore, in closer proximity to mitochondria deep within the muscle fibre (Fig. 2D). Small first instars lack these intracellular tracheoles; however, in large fifth instars, 5% of tracheoles are intracellular. The occurrence of tracheoles that penetrate the surface of other cells has been reported in a number of studies, although they appear to be particularly prevalent in large and highly aerobic flight muscle fibres (Whitten, 1972; Wigglesworth, 1983).

The observation that some tracheoles are functionally intracellular leads to the realisation that the lateral diffusion of oxygen may not be the most appropriate model to apply to tracheoles because it does not account for the extra distance oxygen must travel as it diffuses through the surrounding muscle, or the inevitable dissipation of oxygen molecules as they diffuse further from the tracheole source. In this respect, the flow of oxygen out of tracheoles and into the surrounding muscle in insects is analogous to the flow of oxygen out of capillaries and into the surrounding tissue in vertebrate animals. Therefore, Krogh's cylinder for radial diffusion should offer a more appropriate model on which to estimate the true anatomical conductance for oxygen out of the tracheoles and into the hopping muscle. The results of the present study show that the mean transverse area of muscle serviced by each tracheole is approximately $440\ \mu\text{m}^2$ and this does not vary significantly with increasing body mass. Consequently, the mean maximum distance oxygen must diffuse from a tracheole into the muscle fibre is $\sim 12\ \mu\text{m}$ in locusts at all stages of development. This is comparable to a maximum oxygen diffusion distance of $8\ \mu\text{m}$ in the muscle capillary network of the 2 g Etruscan shrew (Hoppeler et al., 1981b). From the estimate of maximum diffusion distance, it was calculated that the tracheole radial diffusing capacity scales with an exponent of 0.99 (Fig. 3J), which is congruent with both the tracheole lateral diffusing capacity and the aerobic capacity of the hopping muscle. The matching between anatomical tracheole diffusing capacity and the aerobic capacity of the hopping muscle is evidence of symmorphosis in the insect tracheal system, and complements the results of an earlier ontogenetic study on American locusts, which showed that the convective capacity of large tracheae located between the spiracles and the digestive tract matches the metabolic rate of locusts shortly after feeding (Harrison et al., 2005).

Oxygen partial pressure in the terminal tracheoles

By combining the aerobic capacity of the juvenile hopping muscles ($\dot{M}_{\text{O}_2, \text{juv. hop}}$; $\mu\text{mol O}_2\ \text{h}^{-1}$) with the radial diffusing capacity of the tracheoles ($G_{\text{R, trachI}}$; $\mu\text{mol O}_2\ \text{kPa}^{-1}\ \text{h}^{-1}$), and assuming that during strenuous jumping exercise the partial pressure of oxygen in the hopping muscle ($P_{\text{O}_2, \text{muscle}}$) at the furthest average distance from a tracheole is 0.1 kPa, the average partial pressure of oxygen in the tracheoles ($P_{\text{O}_2, \text{trachI}}$) can be calculated according to Fick's law of diffusion:

$$P_{\text{O}_2, \text{trachI}} = (\dot{M}_{\text{O}_2, \text{juv. hop}} / G_{\text{R, trachI}}) + P_{\text{O}_2, \text{muscle}} \approx 17\ \text{kPa}. \quad (23)$$

The average oxygen partial pressure in the terminal tracheoles required to overcome the diffusion barrier and meet the oxygen needs of the hopping muscle during heavy exercise is approximately 17 kPa at 35°C or, expressed as an allometric equation, $P_{\text{O}_2, \text{trachI}} = 19M_b^{0.05 \pm 0.15}\ \text{kPa}$ at 35°C ($r^2 = 0.08$, $N = 9$). It is not possible to measure directly the partial pressure of oxygen in the terminal tracheoles given their small size ($< 2\ \mu\text{m}$ diameter). However, in resting American locusts, direct measurements in the upper regions of the tracheal system reveal that the partial pressure of oxygen is 19 kPa (Gulinson and Harrison, 1996). Given that oxygen is delivered along the tracheal system in the gas phase, it is reasonable to suspect that there may not be a large pressure drop in oxygen between the upper regions of the tracheal system measured by Gulinson and Harrison (Gulinson and Harrison, 1996) and the terminal tracheoles estimated in the present study. Therefore, our calculated estimate of approximately 17 kPa in the terminal tracheoles seems reasonable.

Critique

Along each step of the oxygen cascade there is matching between the maximum functional rate at which oxygen flows through the respiratory system and the quantitative investment made into the structures of the respiratory system. This provides strong evidence that the insect respiratory system is designed according to the economic principles of symmorphosis. However, it should be recognised that the variation in the scaling exponents for the tracheal system might reduce the power of an ANCOVA to distinguish differences with the scaling of the hopping muscle's aerobic capacity. This variation exists despite the analysis of 108 light micrographs and 1326 electron micrographs from nine individuals spanning a 32-fold range in body mass.

Some of the variation in the tracheal exponents could arise because the allometric equation may not accurately reflect changes in tracheal dimensions that occur during ontogeny. While muscle volume increases continually throughout development, the tracheal system undergoes significant expansion only at moulting (Ryerse and Locke, 1978; Wigglesworth, 1981). Therefore, in reality the dimensions of the tracheal system during ontogeny would likely resemble a series of five instar steps, rather than a straight line, and this has probably led to some of the variation. Taking this into account, it is plausible that the reason the third instar locusts consistently lie below the tracheole regression lines (Fig. 3F–J) could be because they were fixed late in their life stage, when the ratio between muscle and tracheole volume is at its widest. Either way, it is unlikely that the third instars bear a strong influence on the final scaling exponent, given that the allometric slope tends to be more affected by data at the upper and lower regions of the analysed body mass range.

The other point worth considering is that in the adult locust, the flight muscles become functional and the insect is capable of oxygen consumption rates far in excess of those attained during terrestrial locomotion. It is reasonable to argue that symmorphosis might be most evident in respiratory systems geared toward extreme performance, such as insect flight. To this end, we have tested whether the vastly different aerobic metabolic rates attained during hopping and flight in the adult locust is matched by a proportional difference in the amount of respiratory structure in the hopping and flight muscles. The results of this study will be published at a later date.

LIST OF ABBREVIATIONS

G_L	lateral diffusing capacity for O_2 (i.e. lateral conductance)
G_R	radial diffusing capacity for O_2 (i.e. radial conductance)

K	Krogh diffusion coefficient (corrected to 35°C using $Q_{10}=1.1$)
M_b	body mass
$M_{M_{O_2,juv,hop}}$	maximum oxygen consumption rate of juvenile locust hopping muscles
r_{cut}	mean radius to inner surface of tracheole cuticle layer
R_{cut}	mean radius to outer surface of tracheole cuticle layer
R_{epi}	mean radius to outer surface of tracheole epidermal layer
R_{muscle}	mean radius of muscle serviced by each tracheole
S	surface area
S_V	surface area density
T	transverse area
V	volume
V_V	volume density
τ	harmonic mean barrier thickness

ACKNOWLEDGEMENTS

This research was supported by the Australian Research Council, project no. DP0879605. Mr Kerry Gascoigne and Dr Mike Teo of Flinders Microscopy, and Ms Ruth Williams and Ms Lyn Waterhouse of Adelaide Microscopy shared their expertise in the field of electron microscopy, which was greatly appreciated. The authors also thank Prof. Stephen Simpson and Mr Tim Dodgson from the University of Sydney for technical advice and providing the founding locust colony. We also acknowledge two anonymous reviewers who improved an earlier version of this manuscript.

REFERENCES

- Albrecht, F. O. (1953). *The Anatomy of the Migratory Locust*. London: Athlone Press.
- Baddeley, A. J., Gundersen, H. J. G. and Cruz-Orive, L. M. (1986). Estimation of surface area from vertical sections. *J. Microsc.* **142**, 259-276.
- Bartels, H. (1971). Diffusion coefficients and Krogh's diffusion constants. In *Respiration and Circulation* (ed. P. L. Altman and D. S. Dittmer), pp. 21-22. Bethesda, MD: Federation of American Societies for Experimental Biology.
- Bennet-Clark, H. C. (1975). The energetics of the jump of the locust *Schistocerca gregaria*. *J. Exp. Biol.* **63**, 53-83.
- Biserova, N. M. and Pfluger, H. J. (2004). The ultrastructure of locust pleuroaxillary "steering" muscles in comparison to other skeletal muscles. *Zoology* **107**, 229-242.
- Bridges, C. R. and Scheid, P. (1982). Buffering and CO₂ dissociation of body fluids in the pupa of the silkworm moth, *Hyalophora cecropia*. *Respir. Physiol.* **48**, 183-197.
- Canals, M., Figueroa, D. P. and Sabat, P. (2010). Symmorphosis in the proximal pathway for oxygen in the leaf-eared mouse *Phyllotis darwini*. *Biol. Res.* **43**, 75-81.
- Canals, M., Martinez, B. B., Figueroa, D. and Sabat, P. (2011). Adjustments of the oxygen diffusing capacity to energetic demands during the development of the quail (*Coturnix coturnix japonica*). *Comp. Biochem. Physiol.* **159A**, 339-345.
- Chapman, R. F. (1998). *The Insects: Structure and Function*. Cambridge: Cambridge University Press.
- Cruz-Orive, L. M. and Weibel, E. R. (1990). Recent stereological methods for cell biology: a brief survey. *Am. J. Physiol.* **258**, 148-156.
- Diamond, J. M. (1992). The red flag of optimality. *Nature* **355**, 204-206.
- Dudley, R. (1998). Atmospheric oxygen, giant Paleozoic insects and the evolution of aerial locomotor performance. *J. Exp. Biol.* **201**, 1043-1050.
- Dudley, R. and Gans, C. (1991). A critique of symmorphosis and optimality models in physiology. *Physiol. Zool.* **64**, 627-637.
- Gabriel, J. M. (1985a). The development of the locust jumping mechanism: II. Energy storage and muscle mechanics. *J. Exp. Biol.* **118**, 327-340.
- Gabriel, J. M. (1985b). The development of the locust jumping mechanism: I. Allometric growth and its effect on jumping performance. *J. Exp. Biol.* **118**, 313-326.
- Garland, T. and Huey, R. B. (1987). Testing symmorphosis: does structure match functional requirements? *Evolution* **41**, 1404-1409.
- Garland, T. (1998). Conceptual and methodological issues in testing the predictions of symmorphosis. In *Principles of Animal Design: The Optimization and Symmorphosis Debate* (ed. E. R. Weibel, C. R. Taylor and L. Bolis), p. 40-47. Cambridge: Cambridge University Press.
- Gębczyński, A. K. and Konarzewski, M. (2011). Effects of oxygen availability on maximum aerobic performance in *Mus musculus* selected for basal metabolic rate or aerobic capacity. *J. Exp. Biol.* **214**, 1714-1720.
- Gehr, P., Mwangi, D. K., Ammann, A., Maloju, G. M. O., Taylor, C. R. and Weibel, E. R. (1981). Design of the mammalian respiratory system. V. Scaling morphometric pulmonary diffusing capacity to body mass: wild and domestic mammals. *Respir. Physiol.* **44**, 61-86.
- Graham, J. B., Dudley, R., Aguilar, N. M. and Gans, C. (1995). Implications of the late Palaeozoic oxygen pulse for physiology and evolution. *Nature* **375**, 117-120.
- Greenlee, K. J. and Harrison, J. F. (2004). Development of respiratory function in the American locust *Schistocerca americana*: II. Within-instar effects. *J. Exp. Biol.* **207**, 509-517.
- Greenlee, K. J., Henry, J. R., Kirkton, S. D., Westneat, M. W., Fezzaa, K., Lee, W. K. and Harrison, J. F. (2009). Synchrotron imaging of the grasshopper tracheal system: morphological and physiological components of tracheal hypermetry. *Am. J. Physiol.* **297**, 1343-1350.
- Gulinson, S. L. and Harrison, J. F. (1996). Control of resting ventilation rate in grasshoppers. *J. Exp. Biol.* **199**, 379-389.
- Harrison, J. F., Lafreniere, J. J. and Greenlee, K. J. (2005). Ontogeny of tracheal dimensions and gas exchange capacities in the grasshopper, *Schistocerca americana*. *Comp. Biochem. Physiol.* **141A**, 372-380.
- Hartung, D. K., Kirkton, S. D. and Harrison, J. F. (2004). Ontogeny of tracheal system structure: a light and electron-microscopy study of the metathoracic femur of the American locust, *Schistocerca americana*. *J. Morphol.* **262**, 800-812.
- Hoppeler, H., Mathieu, O., Krauer, R., Claasen, H., Armstrong, R. B. and Weibel, E. R. (1981a). Design of the mammalian respiratory system. VI. Distribution of mitochondria and capillaries in various muscles. *Respir. Physiol.* **44**, 97-111.
- Hoppeler, H., Mathieu, O., Weibel, E. R., Krauer, R., Lindstedt, S. L. and Taylor, C. R. (1981b). Design of the mammalian respiratory system. VIII. Capillaries in skeletal muscles. *Respir. Physiol.* **44**, 129-150.
- Howard, C. V. and Reed, M. G. (1998). *Unbiased Stereology: Three-Dimensional Measurement in Microscopy*. Oxford: BIOS Scientific Publishers.
- Hsia, C. C. W., Herazo, L. F. and Johnson, R. L. (1992). Cardiopulmonary adaptations to pneumonectomy in dogs. I. Maximal exercise performance. *J. Appl. Physiol.* **73**, 362-367.
- Jones, J. H. and Lindstedt, S. L. (1993). Limits to maximal performance. *Annu. Rev. Physiol.* **55**, 547-569.
- Kaiser, A., Klok, C. J., Socha, J. J., Lee, W. K., Quinlan, M. C. and Harrison, J. F. (2007). Increase in tracheal investment with beetle size supports hypothesis of oxygen limitation on insect gigantism. *Proc. Natl. Acad. Sci. USA* **104**, 13198-13203.
- Karas, R. H., Taylor, C. R., Jones, J. H., Lindstedt, S. L., Reeves, R. B. and Weibel, E. R. (1987). Adaptive variation in the mammalian respiratory system in relation to energetic demand. VII. Flow of oxygen across the pulmonary gas exchanger. *Respir. Physiol.* **69**, 101-115.
- Kirkton, S. D., Niska, J. A. and Harrison, J. F. (2005). Ontogenetic effects on aerobic and anaerobic metabolism during jumping in the American locust, *Schistocerca americana*. *J. Exp. Biol.* **208**, 3003-3012.
- Kohnert, S., Perry, S. F. and Schmitz, A. (2004). Morphometric analysis of the larval branchial chamber in the dragonfly *Aeshna cyanea* Muller (Insecta, Odonata, Anisoptera). *J. Morphol.* **261**, 81-91.
- Kreuzer, F. (1982). Oxygen supply to tissues: the Krogh model and its assumptions. *Experientia* **38**, 1415-1426.
- Krogh, A. (1919). The number and distribution of capillaries in muscles with calculations of the oxygen pressure head necessary for supplying the tissue. *J. Physiol.* **52**, 409-415.
- Maina, J. N. (1989). Scanning and transmission electron microscopic study of the tracheal air sac system in a grasshopper *Chrotogonus senegalensis* (Kraus) - Orthoptera: Acrididae: Pyrgomorphae. *Anat. Rec.* **223**, 393-405.
- Mathieu, O., Krauer, R., Hoppeler, H., Gehr, P., Lindstedt, S. L., Alexander, R. M., Taylor, C. R. and Weibel, E. R. (1981). Design of the mammalian respiratory system. VII. Scaling mitochondrial volume in skeletal muscle to body mass. *Respir. Physiol.* **44**, 113-128.
- Mayhew, T. M. (1991). The new stereological methods for interpreting functional morphology from slices of cells and organs. *Exp. Physiol.* **76**, 639-665.
- Mizisin, A. P. and Ready, N. E. (1986). Growth and development of flight muscle in the locust (*Schistocerca nitens*, Thunberg). *J. Exp. Zool.* **237**, 45-55.
- Pascoe, J. R., Ferraro, G. L., Cannon, J. H., Arthur, R. M. and Wheat, J. D. (1981). Exercise induced pulmonary hemorrhage in racing thoroughbreds: a preliminary study. *Am. J. Vet. Res.* **42**, 703-707.
- Powers, S. K., Lawler, J., Dempsey, J. A., Dodd, S. and Landry, G. (1989). Effects of incomplete pulmonary gas exchange on VO₂max. *J. Appl. Physiol.* **66**, 2491-2495.
- Queathem, E. (1991). The ontogeny of grasshopper jumping performance. *J. Insect Physiol.* **37**, 129-138.
- Runciman, S., Seymour, R. S., Baudinette, R. V. and Pearson, J. T. (2005). An allometric study of lung morphology during development in the Australian pelican, *Pelecanus conspicillatus*, from embryo to adult. *J. Anat.* **207**, 365-380.
- Ryerse, J. S. and Locke, M. (1978). Ecdysterone-mediated cuticle deposition and the control of growth in insect tracheae. *J. Insect Physiol.* **24**, 541-550.
- Sacktor, B. (1976). Biochemical adaptations for flight in the insect. *Biochem. Soc. Symp.* **41**, 111-131.
- Schmitz, A. and Perry, S. F. (1999). Stereological determination of tracheal volume and diffusing capacity of the tracheal walls in the stick insect *Carausius morosus* (Phasmatodea, Lonchodidae). *Physiol. Biochem. Zool.* **72**, 205-218.
- Schmitz, A. and Perry, S. F. (2001). Bimodal breathing in jumping spiders: morphometric partitioning of the lungs and tracheae in *Salticus scenicus* (Arachnida, Araneae, Salticidae). *J. Exp. Biol.* **204**, 4321-4334.
- Schmitz, A. and Perry, S. F. (2002a). Respiratory organs in wolf spiders: morphometric analysis of lungs and tracheae in *Pardosa lugubris* (L.) (Arachnida, Araneae, Lycosidae). *Arthropod Struct. Dev.* **31**, 217-230.
- Schmitz, A. and Perry, S. F. (2002b). Morphometric analysis of the tracheal walls of the harvestmen *Nemastoma lugubre* (Arachnida, Opiliones, Nemastomatidae). *Arthropod Struct. Dev.* **30**, 229-241.
- Schwerzmann, K., Hoppeler, H., Kayar, S. R. and Weibel, E. R. (1989). Oxidative capacity of muscle and mitochondria: correlation of physiological, biochemical, and morphometric characteristics. *Proc. Natl. Acad. Sci. USA* **86**, 1583-1587.
- Seeherman, H. J., Taylor, C. R., Maloju, G. M. O. and Armstrong, R. B. (1981). Design of the mammalian respiratory system. II. Measuring maximum aerobic capacity. *Respir. Physiol.* **44**, 11-23.
- Seymour, R. S., Runciman, S. and Baudinette, R. V. (2008). Development of maximum metabolic rate and pulmonary diffusing capacity in the superprecocial Australian brush turkey *Alectura lathamii*: an allometric and morphometric study. *Comp. Biochem. Physiol.* **150A**, 169-175.
- Seymour, R. S., Runciman, S., Baudinette, R. V. and Pearson, J. T. (2004). Developmental allometry of pulmonary structure and function in the altricial Australian pelican *Pelecanus conspicillatus*. *J. Exp. Biol.* **207**, 2663-2669.
- Smith, D. S. (1963). The structure of flight muscle sarcosomes in the blowfly *Calliphora erythrocephala* (Diptera). *J. Cell Biol.* **19**, 115-138.
- Smith, J. M. (1978). Optimization theory in evolution. *Annu. Rev. Ecol. Syst.* **9**, 31-56.
- Snelling, E. P., Seymour, R. S., Matthews, P. G. D., Runciman, S. and White, C. R. (2011). Scaling of resting and maximum hopping metabolic rate throughout the life cycle of the locust *Locusta migratoria*. *J. Exp. Biol.* **214**, 3218-3224.

- Suarez, R. K.** (1996). Upper limits to mass-specific metabolic rates. *Annu. Rev. Physiol.* **58**, 583-605.
- Suarez, R. K.** (2000). Energy metabolism during insect flight: biochemical design and physiological performance. *Physiol. Biochem. Zool.* **73**, 765-771.
- Suarez, R. K., Lighton, J. R. B., Brown, G. S. and Mathieu-Costello, O.** (1991). Mitochondrial respiration in hummingbird flight muscles. *Proc. Natl. Acad. Sci. USA* **88**, 4870-4873.
- Taylor, C. R. and Weibel, E. R.** (1981). Design of the mammalian respiratory system. I. Problem and strategy. *Respir. Physiol.* **44**, 1-10.
- Taylor, C. R., Maloiy, G. M. O., Weibel, E. R., Langman, V. A., Kamau, J. M. Z., Seeherman, H. J. and Heglund, N. C.** (1981). Design of the mammalian respiratory system. III. Scaling maximum aerobic capacity to body mass: wild and domestic mammals. *Respir. Physiol.* **44**, 25-37.
- Weibel, E. R.** (1970). Morphometric estimation of pulmonary diffusion capacity. I. Model and method. *Respir. Physiol.* **11**, 54-75.
- Weibel, E. R. and Knight, B. W.** (1964). A morphometric study on the thickness of the pulmonary air-blood barrier. *J. Cell Biol.* **21**, 367-384.
- Weibel, E. R., Taylor, C. R., Gehr, P., Hoppeler, H., Mathieu, O. and Maloiy, G. M. O.** (1981a). Design of the mammalian respiratory system. IX. Functional and structural limits for oxygen flow. *Respir. Physiol.* **44**, 151-164.
- Weibel, E. R., Gehr, P., Cruz-Orive, L. M., Muller, A. E., Mwangi, D. K. and Haussener, V.** (1981b). Design of the mammalian respiratory system. IV. Morphometric estimation of pulmonary diffusing capacity: critical evaluation of a new sampling method. *Respir. Physiol.* **44**, 39-59.
- Weibel, E. R., Taylor, C. R. and Hoppeler, H.** (1991). The concept of symmorphosis: a testable hypothesis of structure-function relationship. *Proc. Natl. Acad. Sci. USA* **88**, 10357-10361.
- Weibel, E. R., Bacigalupe, L. D., Schmitt, B. and Hoppeler, H.** (2004). Allometric scaling of maximal metabolic rate in mammals: muscle aerobic capacity as determinant factor. *Respir. Physiol. Neurobiol.* **140**, 115-132.
- Weis-Fogh, T.** (1967). Respiration and tracheal ventilation in locusts and other flying insects. *J. Exp. Biol.* **47**, 561-587.
- Westneat, M. W., Betz, O., Blob, R. W., Fezzaa, K., Cooper, W. J. and Lee, W. K.** (2003). Tracheal respiration in insects visualized with synchrotron X-ray imaging. *Science* **299**, 558-560.
- Whitten, J. M.** (1972). Comparative anatomy of the tracheal system. *Annu. Rev. Entomol.* **17**, 373-402.
- Wigglesworth, V. B.** (1965). *The Principles of Insect Physiology*. London: Methuen.
- Wigglesworth, V. B.** (1981). The natural history of insect tracheoles. *Physiol. Entomol.* **6**, 121-128.
- Wigglesworth, V. B.** (1983). The physiology of insect tracheoles. *Adv. Insect Physiol.* **17**, 85-148.
- Zar, J. H.** (1998). *Biostatistical Analysis*. Englewood Cliffs, NJ: Prentice Hall.